1. Background: climatic significance of snail $\delta^{13}C_{shell}$ in the EASM region

The shell carbonate of land snails is precipitated from the bicarbonate dissolved in body fluids, in which the primary carbon source is the respired CO_2 derived from the snail's ingested food, most of which is composed of local plants (Goodfriend and Hood, 1983; McConnaughey and Gillikin, 2008). Thus, it is generally agreed that the $\delta^{13}C$ of the plant material ingested by a snail is the dominant control on $\delta^{13}C_{shell}$, which in turn reflects the regional vegetation composition (i.e., C_3, C_4, and CAM) (e.g., Balakrishnan et al., 2005; Stott, 2002), and thus the humidity of the local environment (Prendergast et al., 2017; Yanes et al., 2009). However, $\delta^{13}C_{shell}$ can also be influenced by a snail's environmental carbonate ingestion, atmospheric CO_2, and several eco-physiologically-related factors (i.e., food preference, metabolic rates, and the duration of activity), resulting in a regionally specific relationship between $\delta^{13}C_{shell}$ and environmental variables (Balakrishnan, M., and Yapp, 2004; Bao et al., 2018; Goodfriend and Ellis, 2002; Wang et al., 2019). Therefore, it is necessary to evaluate the climatic significance of $\delta^{13}C_{shell}$ in the EASM region before using it for paleoclimatic reconstruction.

Our previous studies have confirmed that $\delta^{13}C_{shell}$ in the EASM region is an indicator of EASM intensity, especially precipitation amount (Bao et al., 2018; 2019). Specifically, Bao et al. (2018) first observed that the $\delta^{13}C_{shell}$ of modern snails from eastern China becomes progressively depleted from the semi-arid north to the warm and wet south, as the EASM intensifies. Subsequently, Bao et al. (2019) established a modern calibration equation between $\delta^{13}C_{shell}$ and mean annual precipitation using snail isotopic data from eastern and mid-latitude China (Fig. S1a) and proposed a conceptual

model specifying the mechanism by which precipitation determines $\delta^{13}C_{shell}$. Briefly, precipitation amount controls $\delta^{13}C_{shell}$ via its effect on the $\delta^{13}C$ values of C_3 plants, snail metabolism, and environmental carbonate leaching, all of which cause changes in $\delta^{13}C_{shell}$ in the same direction, although the latter two processes do not always occur (Fig. S1b; see details in Bao et al., 2019). This is supported by several other studies from the monsoon regions of China. For example, Wang et al. (2019) found that $\delta^{13}C_{shell}$ in *Bradybaena* snails throughout China reflects the $\delta^{13}C$ of regional C_3 plants controlled by rainfall amount, confirming the use of $\delta^{13}C_{shell}$ as a precipitation proxy.

It should be noted that the precipitation data used to correlate $\delta^{13}C_{shell}$ values from above modern calibrations are often the mean annual total, rather than the summer monsoon precipitation. Although at the present-day, the annual precipitation in Xifeng is largely determined by the summer monsoon precipitation, it needs to be determined that this was also the case in the past. We address this issue, as follows. First, modern observations show that, spatially, the proportion of monsoon precipitation accounting for the annual total increases with increasing proximity to the monsoon marginal zone (i.e., ~60–70% in the southeastern Chinese Loess Plateau and > 80% in the northwestern Chinese Loess Plateau). The EASM intensity during glacial stages was weaker than that during interglacial stages; for example, Yang et al. (2015) showed that the northwesterly monsoon rain belt advanced by ~300 km during the warm Holocene compared with the cold LGM (Last Glacial Maximum). These indicate that the proportion of summer monsoon precipitation during glacial periods was higher than that during the Holocene and at the present-day. Second, the ratio of winter precipitation

to summer precipitation in the past can be calculated by analyzing the $\delta^{18}O$ values of samples along fossil shell growth axes (Wang et al., 2020). Based on the criterion of shell $\delta^{18}O$ showing significantly lower values in warm season and higher values in cold season, Wang et al. (2020) divided the snail's growing sections of winter and summer season within a single shell, and showed that the winter precipitation made only a minor contribution to the annual total since the deposition of the L9 loess layer in the Xifeng section. Based on these observations, we consider that our $\delta^{13}C_{shell}$ record mainly reflects variations in summer monsoon precipitation during both glacials and interglacials.

2. Materials and methods

Geological and environmental of the Xifeng section.

We selected the $\delta^{13}C_{shell}$ record of the Xifeng section, in the central Chinese Loess Plateau, mid-latitude China, to reconstruct EASM changes. This is because snail fossils are relatively abundant in the section and numerous comparable paleomonsoon records are also available, as well as a well-constrained chronological framework. Details of the pedostratigraphy of the Xifeng section are given in Sun et al. (1998). In this section the mass accumulation rate (MAR) during glacial intervals was more variable and around two times higher than that during interglacial intervals (Sun and An, 2005).

The climate of the Xifeng area is significantly influenced by the East Asian monsoon system. The winter is generally cold and dry and the summer is warm and humid. The modern mean annual temperature, precipitation, relative humidity, and evaporation are 9.2 ℃, 527.6 mm, 62%, and 520 mm, respectively (Fig. 1b) (Monthly

data are available from the database of the China Meteorological Data Network (http://www.cma.gov.cn/2011qxfw/2011qsjgx/), covering the period of 1981–2010). The Xifeng area is characterized by a semi-arid temperate grassland ecosystem (Hou, 1988), with a relatively simple vegetation composition dominated by C_3 plants, including trees (e.g., *Populus* and *Robinia pseudoacacia Linn.*), shrubs (e.g., *Ziziphus jujuba Mill. var. spinosa (Bunge) Hu ex H.F. Chow*, and *Hippophae rhamnoides Linn.*), and herbs (e.g., *Stephanachne pappophorea* (Hack.) Keng, *Agropyron* and *Pennisetum centrasiaticum Tzvel.*).

Sample pre-treatment, measurements, and data analysis

Snail species identifications were based on shell morphology observed under a binocular microscope. After identification, snail fossil shells were disaggregated into several large pieces and ultrasonically rinsed in deionized water. After drying, the cleaned shell pieces were ground into a powder and then treated with 10% H_2O_2 at 25°C for ~48 h to remove organic matter. $\delta^{13}C_{shell}$ was measured using a Finnigan Delta Plus XP stable isotope mass spectrometer coupled with the Gas Bench II online sample preparation device. The data are reported using the δ notation with reference to the Vienna-Pee Dee Belemnite (V-PDB). Magnetic susceptibility was measured using a Bartington MS2 susceptibility meter.

Additionally, we randomly selected several fossil shells from different depths in the section to conduct mineral morphological analyses using an X-ray diffractometer (XRD) (Rigaku DMAX-IIIA, Japan) at 30 mA and 40 kV, with a curved graphite monochromator with Cu-Kα radiation. Field Emission Scanning Electron Microscopy

(FE-SEM, Zeiss Sigma 500) was also applied to determine the mineral morphology of the shell carbonate. The XRD and SEM results indicate that the primary aragonite of the shells has not been altered to calcite by diagenesis (Fig. S2).

To characterize the spectral characteristics of the $\delta^{13}C_{shell}$ time series, we conducted wavelet and power spectral analyses using Matlab 2012a, after linear interpolation of the time series to a 1-kyr interval. Additionally, cross-spectral analysis was performed to examine the coherence and phase relationship between different proxy records. Monte Carlo methods were used to assess red noise backgrounds to determine the statistical significance of the results.

Possible effects of species on isotopic compositions

The snail assemblage of the Xifeng section is mainly composed of *Cathaica orithyia*, *Metodontia huaiensis* and *Cathaica pulveratricula* (Fig. S2c). *Cathaica orithyia* is the dominant species and it is almost continuously present from the L5 loess layer upwards; while *Cathaica pulveratricula* is common in the transition periods between glacials and interglacials, such as the transitions of L2/S1, L4/S3 and L5/S4. *Metodontia huaiensis* is often present in older strata (i.e., in L4, S4 and L5), except for the bottom part of L2 (Fig. S3a). Several previous studies claimed that different snail species may show distinct isotope compositions due to different eco-physiological factors (e.g., Bao et al., 2018). To assess such possible species effects, fossil shells in some units where two or more species coexisted were selected for carbon isotope analysis. The T-test results (Table S1) indicated no significant differences in $\delta^{13}C_{shell}$ among different species, which enabled us to combine different species to evaluate the

response of shell isotopic compositions to climate changes on the orbital scale.

Isotopic variations among snail individuals from a single sample

We selected snails collected from the depths of 7.7, 17.9 and 38.6 m, for which the numbers of analyzed snails exceeded 10, to evaluate $\delta^{13}C_{shell}$ variations among snails from a single sampling unit. The ranges of $\delta^{13}C_{shell}$ variation for these three depths are: -10.36‰ to -5.06‰ (mean±1σ: -7.79±1.53‰), -8.17‰ to -3.81‰ (mean±1σ: -6.22±1.31‰) and -7.84‰ to -5.71‰ (mean±1σ: -6.64±0.76‰), respectively. Additionally, we found a total of 45 samples containing 3 or more snails, and their average $\delta^{13}C_{shell}$ range within a sampling unit was ~2‰. This amplitude of fluctuation is common, and it is insufficient to affect the reliability of $\delta^{13}C_{shell}$ as a climatic indicator. This is because numerous calibration studies (e.g., Goodfriend and Ellis, 2002; Yanes et al., 2009; Bao et al., 2019; 2020) have found that the mean $\delta^{13}C_{shell}$ values of a site were significantly correlated with environmental or climatic parameters, although the range of variation of $\delta^{13}C_{shell}$ within snail populations at a single site is comparable or even larger than that in a sampling unit of the present study.

Chronological framework

Loess chronologies are mainly generated using three tuning methods: 1) tuning the loess grain-size or magnetic susceptibility record to lagged precession and obliquity curves (e.g., Ding et al., 2002; Sun et al., 2006; Lu et al., 2021); 2) correlating loess proxies with benthic foraminiferal $\delta^{18}O$ records (e.g., Hao et al., 2012; Sun et al., 2019); 3) matching loess proxies with speleothem $\delta^{18}O$ records (e.g., Wang et al., 2021; Sun et al., 2021). These approaches result in almost identical ages of the loess/paleosol

boundaries from S8 to S0, and the age differences among them for most glacial terminations are ~2– 4 kyr (Sun et al., 2019; Sun et al., 2021).

In this study we used the method of Sun et al. (2006) to construct the chronology. This was because the proxy time series of Sun et al. (2006) is based on the samples from the same section (the Zhaojiachuan section in the Xifeng area) as we used, and their age model is the most representative chronological framework for the Xifeng section and has been successfully applied to other loess sections, such as Lingtai (Sun et al., 2010). Sun et al. (2006) directly tuned mean grain size records to orbital obliquity and precession, and then generated mean grain size and magnetic susceptibility time series. Importantly, they found that the two resulting time series were well correlated, and thus the chronological framework for our $\delta^{13}C_{shell}$ record could be constructed based on correlating our magnetic susceptibility record to the magnetic susceptibility time series of Sun et al. (2006), because of the strong similarity of these two signals (Fig. S3b and c). Specifically, using AnalySeries software (Paillard et al., 1996), the magnetic susceptibility record of Sun et al. (2006) was used as the target curve for our magnetic susceptibility record. The tie points selected for the initial correlation of these two magnetic-susceptibility curves are often the midpoint between the start and end of an interval of rapid change in the respective magnetic susceptibility proxy records (diamond labels in Fig. S3). The fundamental requirement for selecting tie points was to ensure that the sedimentation rates did not change excessively.

The reliability of our resulting age model is confirmed by the following observations. First, the transition times in our age model are highly consistent with the

timing of the glacial/interglacial transitions of a benthic $\delta^{18}O$ stack (Fig. S3). Second, the magnetic susceptibility records constructed from our age model are generally consistent with those of the most commonly used age models in loess research, revealing good correspondences between loess and paleosol layers (Fig. S4). Moreover, the age differences, if any, among different age models are generally several kyr. (Fig. S4). It is important to emphasize that the uncertainties in our chronology are insufficient to affect the results of time series analysis of the proxy records on orbital timescales, even precessional. This is because a 23-kyr cyclicity was observed in the leaf wax δD and loess carbonate $\delta^{13}C$ records, for which the chronologies were constructed using one of the abovementioned tuning methods (Wang et al., 2021; Sun et al., 2021). Finally and importantly, the spectral characteristics of the $\delta^{13}C_{shell}$ record exhibit strong 100-kyr cyclicity (mainly concerned in this study) with almost no precessional or obliquity variance, irrespective of the age model used (Fig. S4). This suggests that age model selection does not affect our conclusions.

Reference:

Balakrishnan, M., and Yapp, C. J., 2004, Flux balance models for the oxygen and carbon isotope compositions of land snail shells: Geochimica et Cosmochimica Acta, v. 68, no. 9, p. 2007-2024.

Balakrishnan, M., Yapp, C. J., Theler, J. L., Carter, B. J., and Wyckoff, D. G., 2005, Environmental significance of $^{13}C/^{12}C$ and $^{18}O/^{16}O$ ratios of modern land-snail shells from the southern great plains of North America: Quaternary Research, v. 63, p. 15-30. https://doi.org/10.1016/j.yqres.2004.09.009.

Bao, R., Sheng, X., Li, C., Shen, H., Tan, L., Sun, L., Li, C., Peng, H., Luo, L., Wu, M., Lu, H., Ji, J., and Chen, J., 2020, Effect of altitude on the stable carbon and oxygen isotopic compositions of land snails at the margin of the East Asian monsoon: Geochimica et Cosmochimica Acta, v. 273, p. 99-115.

Bao, R., Sheng, X., Lu, H., Li, C., Luo, L., Shen, H., Wu, M., Ji, J., and Chen, J., 2019, Stable carbon and oxygen isotopic composition of modern land snails along a precipitation gradient in the mid-latitude East Asian monsoon region of China: Palaeogeography, Palaeoclimatology, Palaeoecology, v. 533, p. 109236. https://doi.org/10.1016/j.palaeo.2019.109236.

Bao, R., Sheng, X., Teng, H. H., and Ji, J., 2018, Reliability of shell carbon isotope composition of different land snail species as a climate proxy: A case study in the monsoon region of China: Geochimica et Cosmochimica Acta, v. 228, p. 42-61. https://doi.org/10.1016/j.gca.2018.02.022.

Cheng, H., Edwards, R. L., Sinha, A., Spötl, C., Yi, L., Chen, S., Kelly, M., Kathayat,

G., Wang, X., Li, X., Kong, X., Wang, Y., Ning, Y., and Zhang, H., 2016, The Asian monsoon over the past 640,000 years and ice age terminations: Nature, v. 534, no. 7609, p. 640-646.

Ding, Z. L., Derbyshire, E., Yang, S. L., Yu, Z. W., Xiong, S. F., and Liu, T. S., 2002, Stacked 2.6-Ma grain size record from the Chinese loess based on five sections and correlation with the deep-sea $\delta^{18}O$ record: Paleoceanography, v. 17, no. 3, p. 5-1-5-21.

Goodfriend, G. A., and Ellis, G. L., 2002, Stable carbon and oxygen isotopic variations in modern *Rabdotus* land snail shells in the southern Great Plains, USA, and their relation to environment: Geochimica Et Cosmochimica Acta, v. 66, no. 11, p. 1987-2002.

Goodfriend, G. A., and Hood, D. J., 1983, Carbon Isotope Analysis of Land Snail Shells: Implications for Carbon Sources and Radiocarbon Dating: Radiocarbon, v. 25, no. 3, p. 184–191.

Hao, Q., Wang, L., Oldfield, F., Peng, S., Qin, L., Song, Y., Xu, B., Qiao, Y., Bloemendal, J., and Guo, Z., 2012, Delayed build-up of Arctic ice sheets during 400,000-year minima in insolation variability: Nature, v. 490, p. 393-396. https://doi.org/10.1038/nature11493.

Hou, X.Y., 1988 Chinese Vegetation Geography. Beijing: Science Press.

Lisiecki, L. E., and Raymo, M. E., 2005, A Pliocene-Pleistocene stack of 57 globally distributed benthic $\delta^{18}O$ records, v. 20. https://doi.org/10.1029/2004PA001071.

Lu, H., Wang, X., Wang, Y., Zhang, X., Yi, S., Wang, X., Stevens, T., Kurbanov, R., and

Markovic, S., 2021, Chinese loess and the Asian monsoon: What we know and what remains unknown: Quaternary International.

Mcconnaughey, T. A., and Gillikin, D. P., 2008, Carbon isotopes in mollusk shell carbonates: Geo-Marine Letters, v. 28, no. 5, p. 287-299.

Paillard, D., Labeyrie, L., and Yiou, P., 1996, Macintosh Program performs time-series analysis: Eos, Transactions American Geophysical Union, v. 77, no. 39, p. 379-379.

Prendergast, A., Stevens, R.E., Hill, E.A., Barker, G., Hunt, C.O., Oconnell, T.C., 2017, Carbon isotope signatures from land snail shells: Implications for palaeovegetation reconstruction in the eastern Mediterranean: Quaternary International, v. 432, p. 48–57.

Stott, L. D., 2002, The influence of diet on the $\delta^{13}C$ of shell carbon in the pulmonate snail *Helix aspersa*: Earth and Planetary Science Letters, v. 195, no. 3, p. 249-259.

Sun, D., An, Z., Shaw, J., Bloemendal, J. and Sun, Y., 1998, Magnetostratigraphy and palaeoclimatic significance of Late Tertiary aeolian sequences in the Chinese Loess Plateau. Geophysical Journal International: v. 134, p. 207-212.

Sun, Y., An, Z., Clemens, S. C., Bloemendal, J., and Vandenberghe, J., 2010, Seven million years of wind and precipitation variability on the Chinese Loess Plateau: Earth and Planetary Science Letters, v. 297, no. 3, p. 525-535.

Sun, Y., and An, Z., 2005, Late Pliocene-Pleistocene changes in mass accumulation rates of eolian deposits on the central Chinese Loess Plateau: Journal of Geophysical Research: Atmospheres, v. 110, p. 1-8.

https://doi.org/10.1029/2005JD006064.

Sun, Y., Clemens, S. C., Guo, F., Liu, X., Wang, Y., Yan, Y., and Liang, L., 2021, High-sedimentation-rate loess records: A new window into understanding orbital- and millennial-scale monsoon variability: Earth-Science Reviews, v. 220, p. 103731.

Sun, Y., Clemens, S., An, Z., and Yu, Z., 2006, Astronomical timescale and palaeoclimatic implication of stacked 3.6-Myr monsoon records from the Chinese Loess Plateau: Quaternary Science Reviews, v. 25, p. 33-48. https://doi.org/10.1016/j.quascirev.2005.07.005.

Sun, Y., Yin, Q., Crucifix, M., Clemens, S. C., Araya-Melo, P., Liu, W., Qiang, X., Liu, Q., Zhao, H., Liang, L., Chen, H., Li, Y., Zhang, L., Dong, G., Li, M., Zhou, W., Berger, A., and An, Z., 2019, Diverse manifestations of the mid-Pleistocene climate transition: Nature Communications, v. 10, p. 352. https://doi.org/10.1038/s41467-018-08257-9.

Wang, X., Dettman, D. L., Wang, M., Zhang, J., Saito, Y., Quade, J., Feng, S., Liu, J., and Chen, F., 2020, Seasonal wet-dry variability of the Asian monsoon since the middle Pleistocene: Quaternary Science Reviews, v. 247, p. 106568.

Wang, X., Zhai, J., Cui, L., Zhang, S., and Ding, Z., 2019, Stable carbon and oxygen isotopes in shell carbonates of modern land snails in China and their relation to environment variables, v. 124, no. 11, p. 3356-3376.

Wang, Z., Liu, W., Wang, H., Cao, Y., Hu, J., Dong, J., Lu, H., Wang, H., Xing, M., and Liu, H., 2021, New chronology of the Chinese loess-paleosol sequence by leaf wax δD records during the past 800 k.y: Geology.

Yanes, Y., Romanek, C. S., Delgado, A., Brant, H. A., Noakes, J. E., Alonso, M. R., and Ibáñez, M., 2009, Oxygen and carbon stable isotopes of modern land snail shells as environmental indicators from a low-latitude oceanic island: Geochimica Et Cosmochimica Acta, v. 73, no. 14, p. 4077-4099.

Yang, S., Ding, Z., Li, Y., Wang, X., Jiang, W., and Huang, X., 2015, Warming-induced northwestward migration of the East Asian monsoon rain belt from the Last Glacial Maximum to the mid-Holocene: Proceedings of the National Academy of Sciences, v. 112, p. 13178-13183.

FIGURE CAPTIONS

Fig. S1 (a) Shell $\delta^{13}C$ of modern land snails in the EASM regions of China *versus* mean annual precipitation. Light grey points indicate individual data values (n=888) at each sampling site, and red points represent the site-averaged values (n=74). Error bars are one standard deviation of the mean (data are from Bao et al., 2018, 2019). **(b)** Conceptual model describing the mechanism responsible for the precipitation control of the $\delta^{13}C$ of land snail shells in the East Asian monsoon regions, which involves primary (solid arrow) and potential (dotted arrow) processes.

Fig. S2: **(a)** X-ray powder diffraction (XRD) patterns of fossil snail shells from different depths within the Xifeng section. The triangles represent the XRD peak of the pure aragonite standard sample, and depth information is given on the right side of the graph. **(b)** Scanning electron microscope (SEM) image of the needle-column microstructure of fossil snail shell carbonate (randomly selected from a certain depth). Both the XRD and SEM data indicate that the primary aragonite of the shells has not been diagenetically altered. **(c)** Photos of snail fossils used in this study (1: *Cathaica orithyia*; 2: *Cathaica pulveratricula* 3: *Metodontia huaiensis*).

Fig. S3 (a) Shell $\delta^{13}C$ record on a depth scale. Dots with different colors represent all individual snail samples from the three dominant species (grey: *Cathaica orithyia*; brown: *Metodontia huaiensis*; green: *Cathaica pulveratricula*). The curve is based on the mean value in each sampling unit. **(b-c)** Magnetic susceptibility (MS) record on a depth scale. Red diamonds indicate the tie points linking rapid changes in our MS record (brown) with the target MS record from Sun et al. (2006) (blue). **(d-f)** Comparisons of the Xifeng MS and grain-size time-series based on the orbitally-tuned age model of Sun et al. (2006) with the LR04 benthic $\delta^{18}O$ stack (Lisiecki and Raymo, 2005). Dashed lines denote that the chronology was generated by matching the timing of five loess marker layers in our MS record to the MS and grain-size time series of Sun et al. (2006). Grey bars indicated the correlation of paleosol units to interglacial stages.

Fig. S4 (a) Magnetic susceptibility (MS) record from this study (brown circles in each panel) tuned to different age models. The age models from top to bottom are derived from Hao et al. (2012), Wang et al. (2021), Sun et al. (2021), Lu et al. (2021), and Sun et al. (2006), respectively. The chronological model derived from Sun et al. (2006) was selected in this study. The MS or grain size records from the respective studies are also shown (blue circles in each panel). The grey vertical bands represent paleosol layers. **(b)** From top to bottom: spectral and wavelet results of the $\delta^{13}C_{shell}$ record based on different age models corresponding to a.

Fig. S5 Wavelet coherences between the land snail shell $\delta^{13}C$ ($\delta^{13}C_{shell}$) record and other records. (**a**) Xifeng magnetic susceptibility (MS; Sun et al., 2006). (**b**) Jingyuan loess inorganic carbonate $\delta^{13}C$ ($\delta^{13}C_{IC}$; Sun et al., 2019). (**c**) Xifeng plant wax δD (δD_{wax}; Wang et al., 2021). (**d**) Sanbao speleothem $\delta^{18}O$ (Cheng et al., 2016), (**e**) Benthic $\delta^{18}O$ stack (Lisiecki and Raymo, 2005), and (**f**) Xifeng mean grain size (MGS; Sun et al., 2006). Red contours indicate coherence above the 5% significance level.

Fig. S6 Wavelet and spectral analysis results of the mass accumulation rates of eolian deposits on the central Chinese Loess Plateau. Data are from Sun and An (2005).

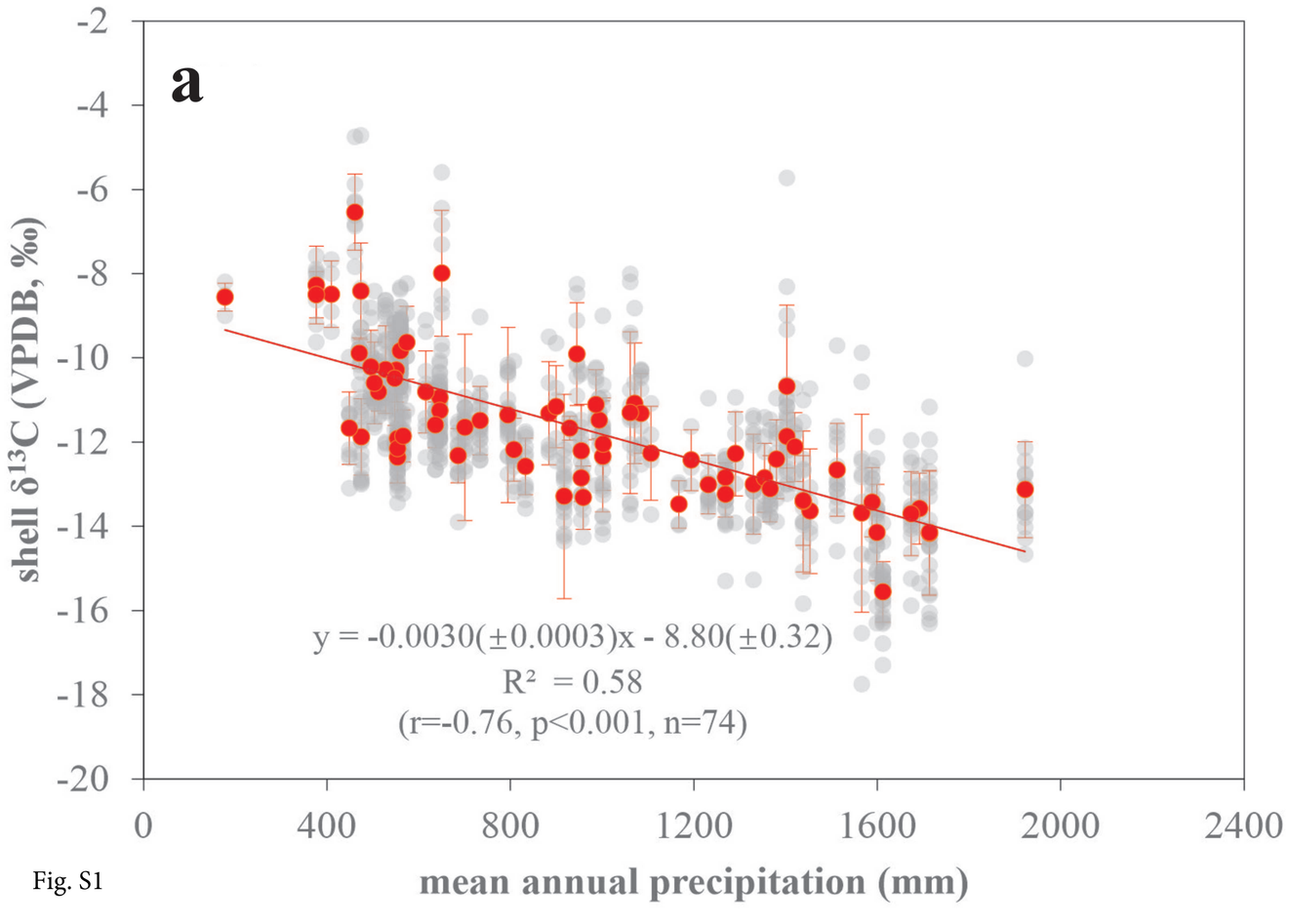
a
shell δ13C (VPDB, ‰)
-2
-4
-6
-8
-10
-12
-14
-16
-18
-20
0
400
800
1200
1600
2000
2400
mean annual precipitation (mm)
y = -0.0030(±0.0003)x - 8.80(±0.32)
R² = 0.58
(r=-0.76, p<0.001, n=74)

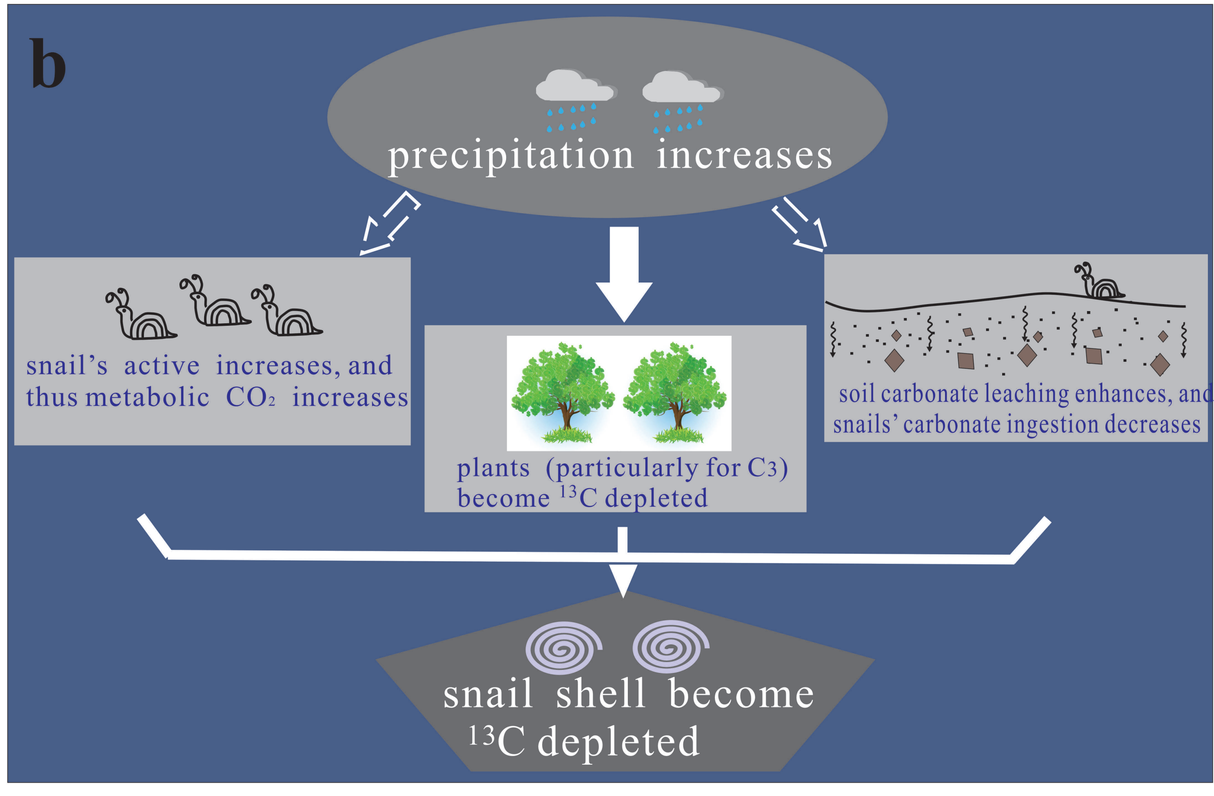
b
precipitation increases
snail's active increases, and thus metabolic CO2 increases
plants (particularly for C3) become 13C depleted
soil carbonate leaching enhances, and snails' carbonate ingestion decreases
snail shell become 13C depleted

Fig. S1

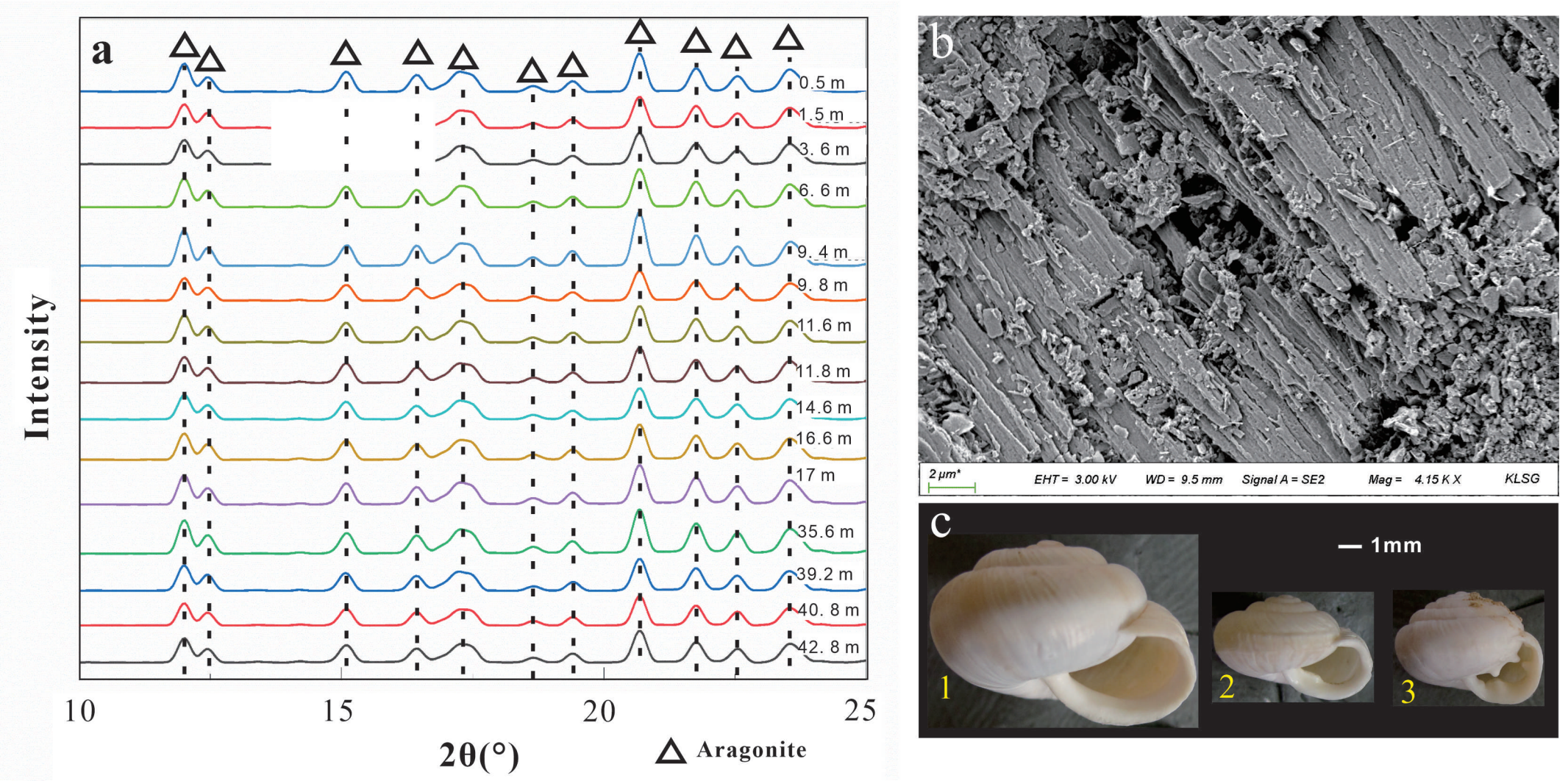
a
0.5 m
1.5 m
3. 6 m
6. 6 m
9. 4 m
9. 8 m
11.6 m
11.8 m
14.6 m
16.6 m
17 m
35.6 m
39.2 m
40. 8 m
42. 8 m
Intensity
10
15
20
25
2θ(°)
Aragonite
b
2 μm*
EHT = 3.00 kV
WD = 9.5 mm
Signal A = SE2
Mag = 4.15 K X
KLSG
c
— 1mm
1
2
3

Fig. S2

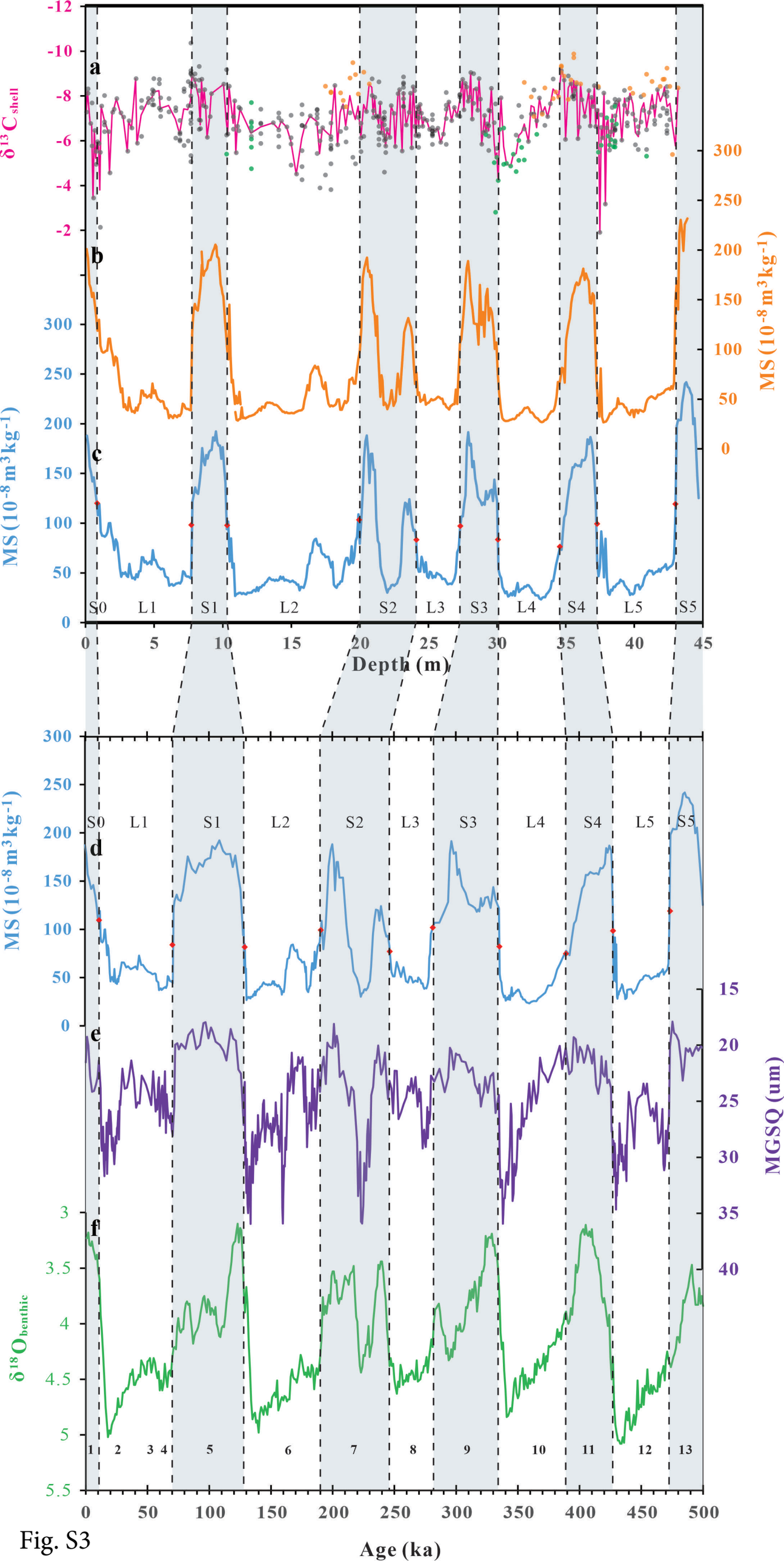
a
b
c
d
e
f
δ13Cshell
MS (10-8 m3kg-1)
Depth (m)
S0
L1
S1
L2
S2
L3
S3
L4
S4
L5
S5
δ18Obenthic
MGSQ (um)
Age (ka)
1
2
3
4
5
6
7
8
9
10
11
12
13

Fig. S3

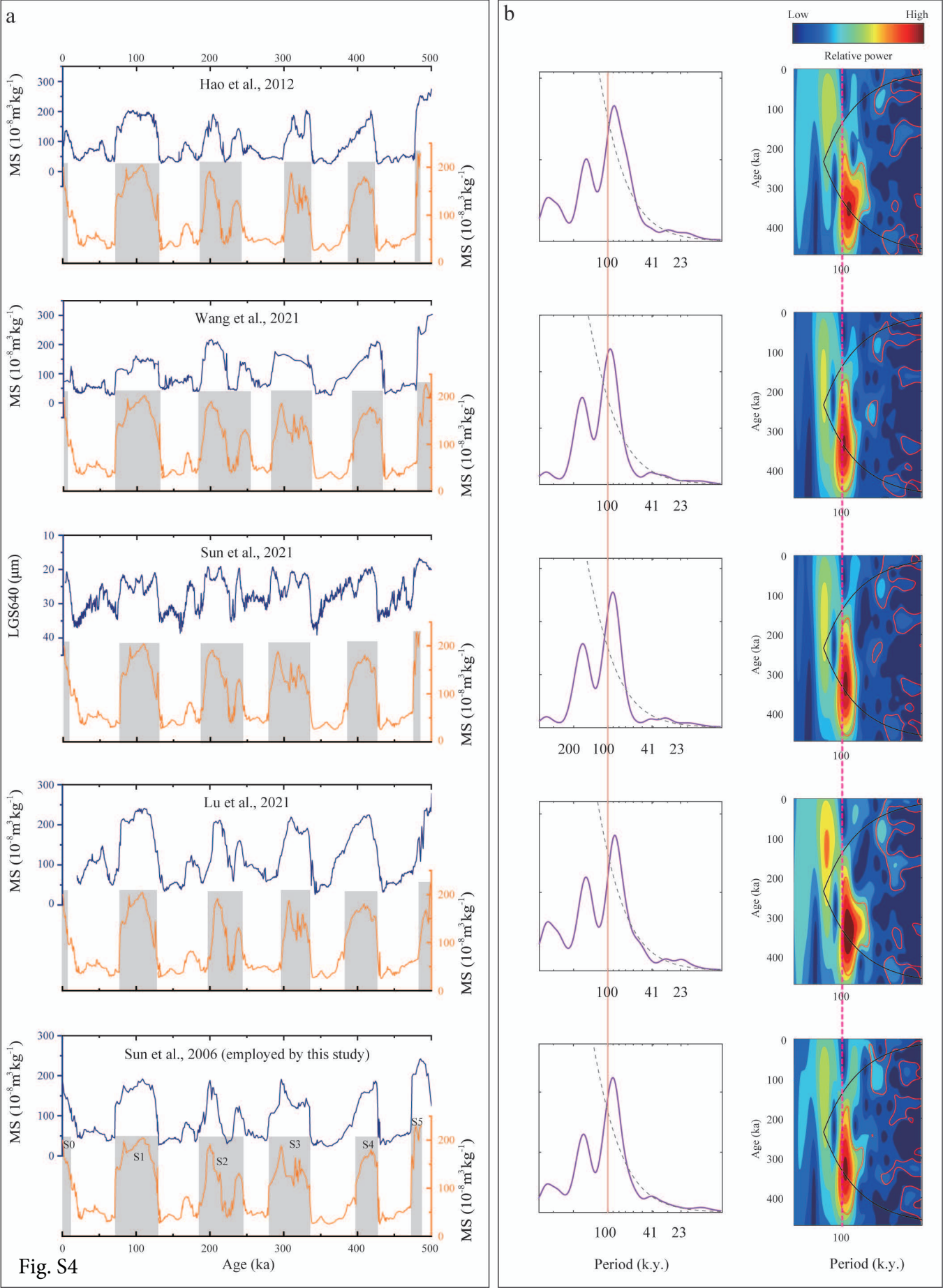
a
b
Hao et al., 2012
Wang et al., 2021
Sun et al., 2021
Lu et al., 2021
Sun et al., 2006 (employed by this study)
MS (10^{-8}m^{3}kg^{-1})
LGS640 (μm)
S0
S1
S2
S3
S4
S5
Age (ka)
Low
High
Relative power
100
41
23
200
Period (k.y.)

Fig. S4

a: $\delta^{13}C_{shell}$ — MS

b: $\delta^{13}C_{shell}$ — $\delta^{13}C_{IC}$

c: $\delta^{13}C_{shell}$ — δD_{wax}

d: $\delta^{13}C_{shell}$ — Speleothem $\delta^{18}O$

e: $\delta^{13}C_{shell}$ — Benthic $\delta^{18}O$

f: $\delta^{13}C_{shell}$ — MGS

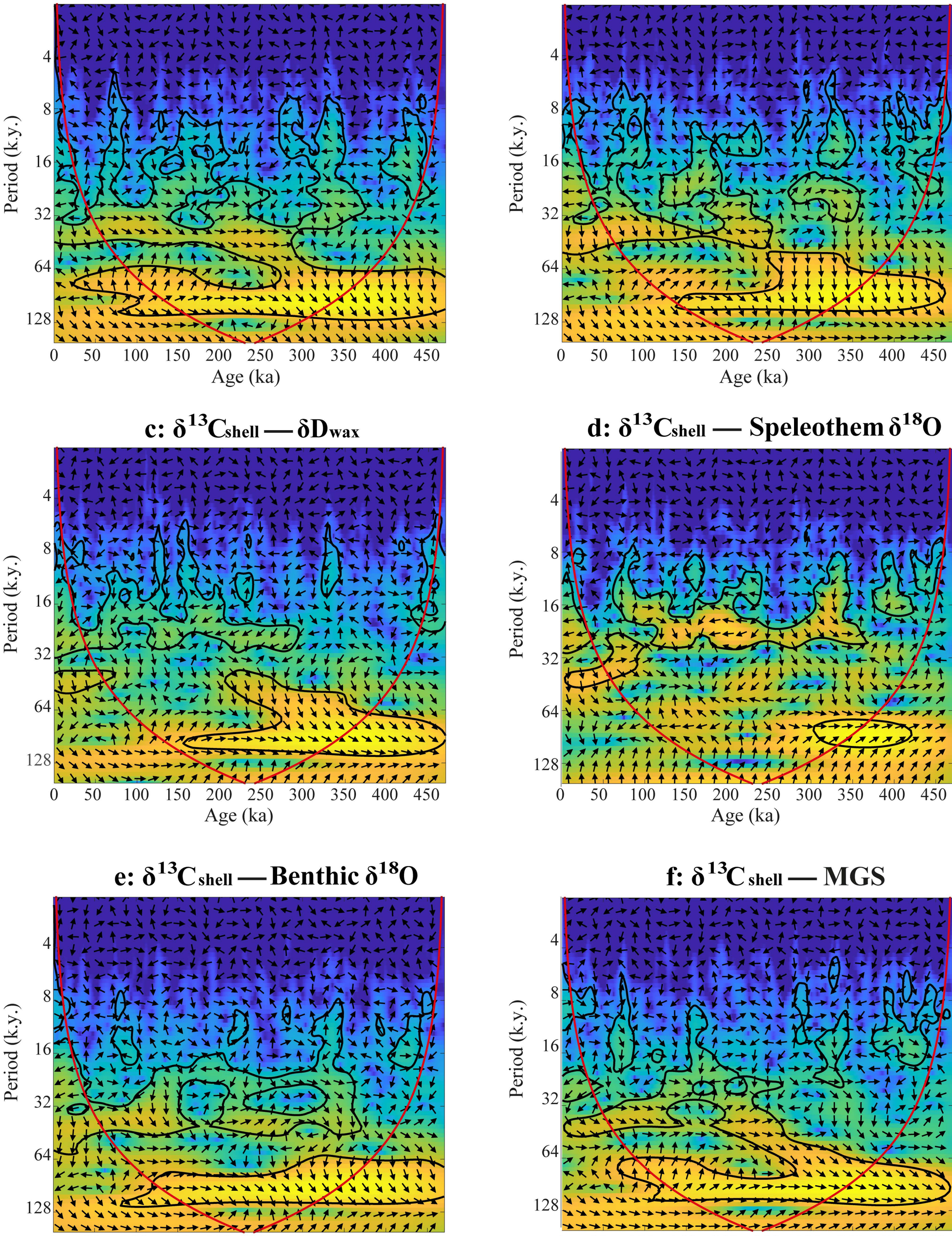

Fig. S5

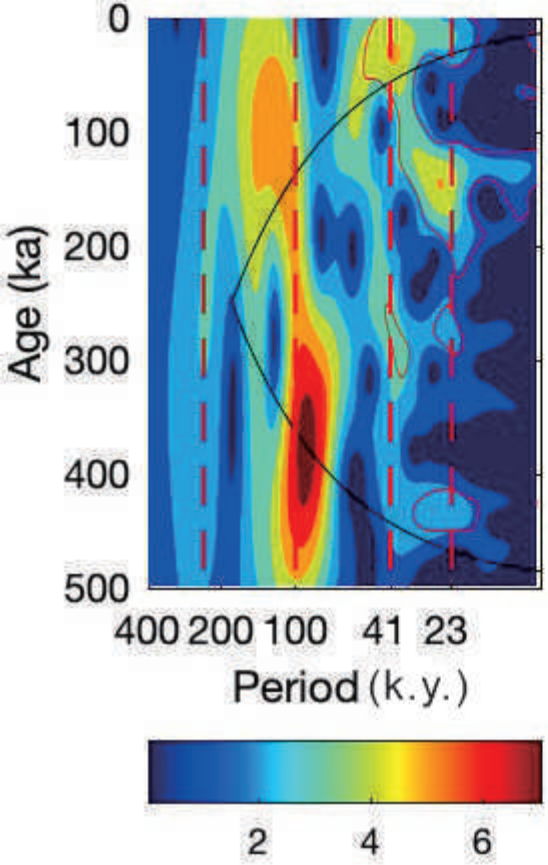
0
100
200
300
400
500
Age (ka)
400 200 100 41 23
Period (k.y.)
2
4
6

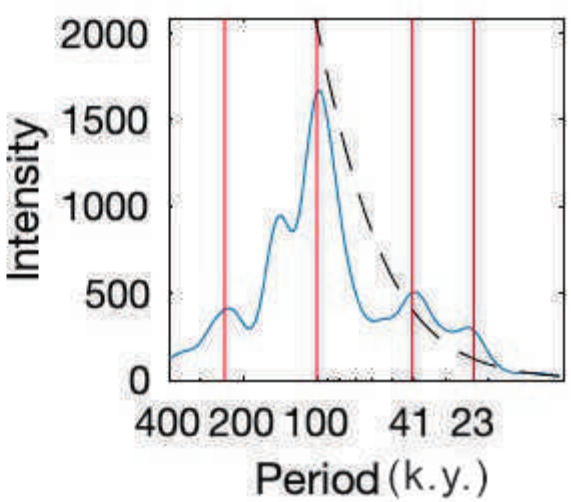
2000
1500
1000
500
0
Intensity
400 200 100 41 23
Period (k.y.)

Fig. S6

Table S1 Variability of carbon isotope values (‰, VPDB) among different snail species by sampling depth. Only species with two or more individuals were included for statistical testing.

Sampling depth	Species	N	Mean $\delta^{13}C_{shell}$	Std	T-test	*p*-Value
12.10 m	*Cathaica orithyia*	3	-6.49	0.34	-0.36	**0.177**
	Cathaica pulveratricula	6	-6.27	1.01		
17.5–20.7 m	*Cathaica orithyia*	24	-6.21	1	6.77	**0.181**
	Metodontia huaiensis	11	-8.42	0.59		

N, number of snail fossil individuals analyzed; std, standard deviation.

Table S2 Carbon isotope values (‰, VPDB) of land snail fossils in loess and paleosol layers of the Xifeng section.

Layer	Age (ka)	Number of samples	Mean $\delta^{13}C$	$\delta^{13}C$ range	Standard deviation
S0	0-12	12	-6.34	4.87	1.40
L1	12.63-74.21	70	-7.33	8.23	1.29
S1	79.46-128.96	20	-7.53	3.91	1.13
L2	130.27-194.80	87	-6.56	5.67	1.12
S2	197.20-246.38	54	-7.14	4.46	1.05
L3	248.08-280.00	40	-6.89	2.45	0.66
S3	286.98-335.05	32	-7.09	6.24	1.36
L4	335.75-395.85	43	-7.07	5.11	1.40
S4	397.51-427.31	25	-7.93	3.82	0.99
L5	427.71-475.92	89	-7.01	7.34	1.18